33rd Annual International Conference of the IEEE EMBS
Boston, Massachusetts USA, August 30 - September 3, 2011

Modeling Study of the Failing Heart and its Interaction with an Implantable Rotary Blood Pump

Deepa P. Ramachandran, Chuan Luo, Tony S. Ma, and John W. Clark, Jr., *Fellow, IEEE*

Abstract—The effectiveness of clinical diagnosis and treatment of heart failure is a direct function of clinical signs that can be measured in a patient within cost and safety constraints. Large-scale mathematical modeling can be a key tool in revealing important, measurable clinical signs of heart failure, furthering medical understanding and development of treatment. In the first part of this study we have created two models of left heart failure – diastolic and systolic, using our human cardiovascular-respiratory system (H-CRS) model, and we present a comparison of the two types with emphasis on novel and differentiating clinical signs, such as tricuspid flow and septal motion. In the event of compromised left ventricular performance, mechanical left ventricular assist devices (LVAD) are often implanted to augment or completely replace the pumping action of the left ventricle (LV). One such type is the implantable rotary blood pump (iRBP). Several design issues related to the iRBP are difficult to study experimentally due to procedure complexity and limitations in animal models of heart failure [2]. Therefore, modeling has become a key tool in iRBP development. In the second part of this study, we have introduced an iRBP model based on [1]-[2] in the systolic failing heart to study the interactions. We consider optimal motor settings for different levels of LV assistance, the effects of the iRBP on the right heart, septum, and pulmonary circulation. Our model results align with those reported in [1]-[2]. Improvement in cardiac output, pulmonary congestion, and heart work are seen with the iRBP. We observe lowered septal assistance to RV and LV ejection with increasing pump speeds, elevating right ventricular (RV) work, reducing LVET, and causing ventricular mechanical dyssynchrony in ejection. These results suggest right heart compromise via the septum's reduced role with the introduction of an iRBP. This work emphasizes the critical role of modeling in heart failure and treatment studies.

Manuscript received April 15, 2011. This work was supported in part by a training fellowship from the Keck Center for Interdisciplinary Bioscience Training of the Gulf Coast Consortia (NLM Grant No. 5T15LM07093).

D. P. Ramachandran is with Rice University, Houston, TX 77005 USA. e-mail: dpr2@rice.edu).

C. Luo was with Rice University, Houston, TX 77005 USA. e-mail: urania@ rice.edu).

T. S. Ma is with Division of Cardiology, VA Medical Center, Houston, TX 77030 USA. e-mail:ma.tonys@va.gov).

J. W. Clark, Jr. is with Rice University, Houston, TX 77005, USA. e-mail:jwc@rice.edu).

I. Introduction

The study of heart failure benefits greatly with the application of mathematical modeling in the practical areas of clinical diagnosis and treatment. The effectiveness of disease diagnosis can be quantified by the relevance of obtainable information on a patient's condition. Large-scale mathematical models of heart failure can point to non-traditional, yet important signs to measure for bettering clinical methods. Modeling is also a key approach in design optimization of left ventricular or bi-ventricular assist devices (LVAD/BiVADs) in treating ventricular failure. For example, operating an LVAD/BiVAD requires consideration of an individual patient's physical variations in cardiovascular parameters. Furthermore, control is necessary to maintain assist device operation as the patient engages in regular activities that create variations in cardiac output (CO) requirements.

Our group has developed a large-scale composite model of the human cardiovascular-respiratory system (H-CRS) that integrates heart mechanics, hemodynamics, circulatory and gas transport aspects of the lung, brain and whole body tissue, and nervous system control of the cardiovascular and respiratory systems into a single large-scale model that can be used to analyze the dynamic behavior of the normal and deranged cardiopulmonary system [3]-[6]. An extensive model such as our H-CRS model provides a broad view of the circulatory, pulmonary, and neural effects important in heart failure and LVAD design studies.

The use of implantable rotary blood pumps (iRBP) as a means of LV assist in the event of LV heart failure is increasing, for multiple reasons. Firstly, iRBP, like other types of ventricular assist devices (VAD), can be used in three modes: a) bridge-to-recovery, wherein the iRBP is implanted short-term to assist the ventricle while the heart is treated for a condition, or during a surgery recovery process, until the heart returns to normal operation and contractility, b) bridge-to-transplant, wherein the VAD is used to keep a patient alive while waiting for a heart transplant, c) destination therapy, wherein a VAD is inserted for long-term use intended for patients who cannot receive a heart transplant (i.e., because of

health ineligibility or age). The benefits of iRBPs are that they can placed inside the chest and that they operate as continuous flow pumps allowing for simpler, smaller, and more reliable designs, as well as reducing the risk of clotting of stagnating blood. The VentrAssist™ iRBP (Ventracor Ltd, Sydney, Australia) has been modeled and studied in [1-2,7], and we have integrated this model in our H-CRS model.

VADs can be operated in two different pumping states depending on the requirement. The first is an assist mode for ventricular ejection (VE), wherein the pump operates in conjunction with the ailing ventricle, to reduce strain on the ventricle, while maintaining ventricular activity. This mode is commonly used in bridge-to-recovery cases, as the minimally working ventricle is allowed time to recuperate and strengthen. The second mode is a replacement mode wherein the pump completely takes over the role of the ventricle and the aortic valve does not open (ANO). For iRBPs, pump speed control is critical in avoiding two dangerous pumping states. The first undesirable state is pump regurgitation (PR) where pump backflow occurs when the speed is too low to drive blood through the aorta. The second dangerous state is ventricular collapse (VC), when the speed is too high causing ventricular walls to collapse and obstruct pump inflow.

VADs are commonly used in cases of heart failure requiring LV systolic assistance. In most cases, this is in the presence of reduced CO due to systolic heart failure (SHF) caused by LV systolic dysfunction (LVSD). LV diastolic dysfunction (LVDD) leading to diastolic heart failure (DHF) is normally not treated with LVADs as the LV volume is already very small, and LVAD assistance shrinks the LV even more. We present a modeling study of both DHF and SHF. Common and novel signs of HF as well as the signs distinguishing the two types are addressed. We then introduce the iRBP in the SHF model to observe the impact. It has been observed that implantation of a LVAD may lead to right heart failure requiring RVAD implantation as well [8], and using our model we make observations on the influence of an LV iRBP on the right heart. We first simulate the four possible operating states. This includes the two desired modes of operation, assist (VE) and replace (ANO), as well as pump regurgitation (PR) and ventricular collapse (VC). Normal heart (NH) and LVSD with no blood pump (NP) are also simulated for comparison. Secondly, we analyze the effects of iRBP on the right heart, septum, neural control, and heart work.

II. Methods

DHF is induced by restrictive-type (R-type) LVDD, wherein the passive stiffness of LV walls is increased. We model R-type LVDD with an increase in the passive stiffness of the LV free wall and septum, increasing the LV diastolic pressures. SHF is modeled by a single-parameter decrease of the end-systolic pressure-volume relationship (ESPVR) slope, which diminishes the systolic pressures and dilates the LV, as is characteristic of SHF. The parameter changes were made such that the stroke volume (SV) decrease was comparable in LVDD and LVSD.

As in [1]-[2], the iRBP can be modeled with three differential equations, the motor windings electrical equation, the electromagnetic torque transfer equation, and the pump hydraulic equation. These three equations define the state variables Q_{BP} (pump flow), ω_{BP} (pump speed), and I_{BP} (motor current).

III. Results

A. Diastolic and Systolic Heart Failure

LVDD and ensuing DHF are characterized by elevated diastolic pressures, lowered SV, high left atrial (LA) pressures due to pulmonary congestion, and normal or near-normal LV ejection fraction (EF) [9]. LVSD and ensuing SHF without remodeling are marked by an enlarged LV, decreased systolic pressures, lowered SV, reduced LVEF, and normal end-diastolic pressure-volume relationship (EDPVR) [9]. Fig. 1 shows P-V loops for both R-type LVDD and LVSD, for the normal (black) and diseased (red) hearts. LVDD increases LV diastolic pressures, reduces end-diastolic volume, and lowers SV (Fig. 1D). LVSD shifts the LV P-V loop far rightward to higher volumes, decreases LV systolic pressure, and lowers SV (Fig. 1H). RV P-V loops in both cases shows higher systolic pressures and delayed pulmonic valve opening (Fig. 1B and F). CO decreases from 4.9 L/min to 3.5 L/min in LVDD and 3.2 L/min in LVSD and pulmonary volume measurements are elevated in comparison to a normal heart (NH) (increases from 562 ml in NH to 708 ml and 661 ml, in LVDD and LVSD, respectively) (Table I). Reflecting these changes, the RA P-V loop shifts downward from normal in both cases due to lowered CO while LA P-V loop shifts upward due to pulmonary congestion. LVEF is near normal in LVDD (drops to 0.65 from 0.72, within 10% of normal), while LVEF is less that 50% in LVSD (0.32) (Table I).

Ratio of the characteristic two peaks (E-wave and A-wave) in mitral and tricuspid flows (Q_M and Q_{TC},

respectively) measured via echocardiography can reveal the presence of diastolic dysfunction. In clinical practice, R-type LVDD is identified by an abnormally high E/A wave Q_M ratio (above the normal range of 1-1.5). Previous work of our group reveals that E/A wave ratio of Q_{TC} is abnormally low regardless of LVDD type [6]. In this work, while Q_M E/A wave ratio rises above normal range in R-type LVDD to 2.67, it is normal in LVSD at 1.15 (Table I). The Q_{TC} E/A wave ratio however, is below normal range in both cases (0.57 with LVDD and 0.56 with LVSD) (Table I). In LVSD, the Q_M ratio does not show abnormality, but similar to the LVDD case, the Q_{TC} ratio is below normal range. Left-sided HF (regardless of LVDD type as well [6]) is revealed consistently in the right heart Q_{TC} E/A wave ratio.

Ventricular mechanical dyssynchrony can be detected in the model by the level of synchrony in inlet and outlet flows from the ventricles. A comparison of transvalvular flows of the right and left of the LVDD study shows that the tricuspid valve is delayed in opening (Fig. 2A2-B2) compared to the synchrony seen in a normal heart (Fig. 2A1-B1). The outlet flows of pulmonary arterial flow (Q_{PA}) and aortic flow (Q_{AO}) are synchronized, with Q_{PA} ending in time with Q_{AO} (Fig. 2C2-D2) unlike the normal heart in which the pulmonic valve closes later (Fig. 2C1-D1). In the LVSD case, while the transvalvular flow synchrony is similar to that of a normal heart (compare Fig. 2A1-B1 with Fig. 2A3-B3), the outlet flows are markedly desynchronized, with a delayed opening of the aortic valve (Fig. 2D3) in comparison to the pulmonic valve (Fig. 2C3). The pulmonic valve also closes earlier than the aortic valve (Fig. 2C3-D3).

B. iRBP Characterization in Presence of LVSD

The iRBP model was integrated with the H-CRS model of LVSD. The iRBP characteristic waveforms are shown in (Fig. 3) for four different pump speeds (1950 rpm, 2000 rpm, 2800 rpm, 3200 rpm) representing operation in the four different modes. Pump regurgitation is seen at very low speeds (1950 rpm) with negative Q_{BP} (Fig. 3A1). The pump operates as expected: with decreasing P_{BP}, I_{BP} and Q_{BP} increase, and vice versa. The motor current (I_{BP}) (Fig. 3A4-D4) and differential pressure (P_{BP}) (Fig. 3A5-D5) steadily rise with greater speeds (ω_{BP}) (Fig. 3A3-D3). At 2000 rpm the pump assists the LV with higher Q_{BP} and reduced LV outflow into the aorta ($Q_{AO,p}$) (Fig. 3B1). The LV contributes much less to ejection with greatly reduced LV ejection time (LVET) (Fig. 3B2 and Table I), and pulse pressure levels off (Fig. 3B2 dotted line) with primary arterial inflow coming from the continuous flow pump. As speed increases, the SV improves. Baroreceptor feedback to this increased SV causes a decrease in heart rate. These model values as well as CO are shown in Table I. At 2800 rpm, the iRBP replaces the LV in its role in ejection. The aortic valve is shut with zero LV outflow (Fig. 3C1 and Table I). LV contraction is minimal and systolic LV pressure is drastically reduced (Fig. 3C2), while on the other hand, RV ejection time (RVET) and CO increase (Table I). Pulse pressure is constant (Fig. 3C2, dotted line). At 3200 rpm, ventricular collapse is observed, as Q_{BP} (Fig. 3D1) drops rapidly at end-systole coincident with P_{LV} falling below zero or collapsing (Fig. 3D2). The sharp changes are observed in I_{BP} (Fig. 3D4) and P_{BP} (Fig. 3D5) waveforms as well.

C. iRBP-H-CRS Model Interactions

iRBP effects on the circulatory loop can be summarized by pressure-volume loops for all four chambers (Fig. 4), featuring the normal heart, heart with LVSD, heart with LVSD and iRBP in VE mode (2000 rpm), and heart with LVSD and iRBP in ANO mode (2800 rpm). LV volume progressively drops with increasing speed (Fig. 4D), and the continuous flow nature of the pump is seen with decreasing volume during LV contraction. In ANO mode, the ventricular systolic pressure is greatly diminished with no LV ejection taking place. On the contrary, end-diastolic RV volume increases with increasing pump speeds to accommodate the increased CO (Fig. 4C). RV systolic pressures drop toward normal. RA pressure increases (Fig. 4A) while LA pressure drops (Fig. 4B) with increasing pump speed, the first reflecting the higher CO, and the second reflecting the lowered pulmonary congestion.

Septal volume (V_{SPT}) plots indicate the change in septal movement (Fig. 5). A positive slope in V_{SPT} indicates rightward movement, whereas a negative slope indicates leftward movement [5]. With LVSD, the septum is rightward bowed through most of diastole due to the characteristically enlarged LV. Septal priming, or the sharp rightward movement at early systole, which aids RV ejection [5]-[6] disappears (Fig. 5C). As a result, the pulmonic valve opens later (A). The following leftward swing is slowed, causing a prolonged LV isovolumic contraction period and delaying the opening of the aortic valve (B). With the iRBP in place, the septal position remains rightward bowed, and the leftward thrust is further slowed. Contrary to the rightward movement during septal priming, the septum shows a slight leftward motion. With increasing pump speed, septal displacement decreases, lessening its critical

role in both RV and LV early ejection. Ejection times are given in Table I - LV ejection time is reduced with iRBP assistance, while the reverse occurs in the RV.

The role and effectiveness of the iRBP can be evaluated through an analysis of total heart work and the contribution of individual elements to work [5]. As shown in Table I, total heart work diminishes with the iRBP in place and at increasing speeds. Fig. 6 displays the work of separate heart components. While PR mode slightly increases left heart work (blue lines in Fig. 6) due to the regurgitant flow, the remaining operating modes VE, ANO and VC cause a marked decrease (95% decrease in W_{LV}, 30% decrease in W_{LA}, Fig. 6A-B), falling far below the control value. On the contrary, RV work rises as pump speed increases (32% increase from control, Fig. 6A, red line), while RA work remains relatively constant (Fig. 6B, red line). Breaking down the work contributions even further, work done by individual ventricular walls is shown in Fig. 6C. LV free wall work decreases (93% below control) and RV free wall work shows no tendency to decrease with pump speed. Septal work (Fig. 6C, black line) decreases by 97%. RV performance as demonstrated by previous work [5-6] is highly dependent on septal contribution particularly during ejection. With septal work at nearly zero, RV work rises.

IV. Discussion

Our H-CRS model has the capability of providing extensive information on heart failure, the operation of an iRBP, and in particular, important signs of right heart effects of LV failure. Novel areas to investigate in heart failure clinical diagnosis are suggested by this work. Our model also suggests new analytical indices such as heart work to improve iRBP design methodologies. Both LVDD and LVSD are simulated, demonstrating the presence of heart failure – most importantly, lowered CO and pulmonary congestion - with the two different types of dysfunction. Other key signs such as consistently abnormal tricuspid flow in LV disease, and ventricular dyssynchrony present at diastole in LVDD and at systole in LVSD are also revealed by the modeling results. A preliminary iRBP design is implemented with demonstration of functionality. The model of SHF can be further improved by introducing diastolic remodeling based on experimental evidence [10] modifying the end-diastolic pressure-volume relationship. The integration of the iRBP serves to improve CO with LVSD in both LV assistance and replacement modes. Left heart work decreases, as is shown with decreased work by the LV free wall, LA and LV, individually. The right heart however, bears an increase in work with the iRBP, a direct result of the reduced septal contribution to RV ejection. The septum has a critical role to play in much of the abnormal ventricular mechanics observed. In summary, the septum in the presence of LVSD creates mechanical ventricular dyssynchrony, delayed LV contraction, reduced RV ejection, and increased RV work. By increasing iRBP speed, there is improvement in SV and CO and reduction in total heart work, but as a drawback, septal assistance to both RV and LV early ejection is further reduced.

V. Conclusions

The H-CRS model developed by our group is well-suited for heart failure and iRBP design studies, with the ability to view right heart effects of a left heart problem, and suggest new clinical diagnostic methods. In addition, analytical indices such as heart work can be beneficial for design.

VI. References

[1] E. Lim, S. Dokos, S.L. Cloherty, R. F. Salamonsen, D.G. Mason, J.A. Reizes, and N.H. Lovell, "Parameter-optimized model of cardiovascular-rotary blood pump interactions," *IEEE Trans. Biomed. Eng.*, vol. 57, no. 2, pp. 254-265, Feb 2010.

[2] E. Lim, S.L. Cloherty, J.A. Reizes, D.G. Mason, R.F. Salamonsen, D.M. Karantonis, and N.H. Lovell, "A dynamic lumped parameter model of the left ventricular assisted circulation," *Proceedings of the 29th Annual International Conference of the IEEE EMBS*, pp. 3990-3, 2007.

[3] K. Lu, J.W. Clark, Jr., F.H. Ghorbel, D.L. Ware, and A. Bidani, "A human cardiopulmonary system model applied to the analysis of the Valsalva maneuver," *Am J Physiol. Heart Circ Physiol.* 2001, 281(6): H2661-79.

[4] C. Luo, D.L. Ware, J.B. Zwischenberger, J.W. Clark, Jr., "Using a human cardiopulmonary model to study and predict normal and diseased ventricular mechanics, septal interaction, and atrio-ventricular blood flow patterns," *J Cardiovasc Engineering* 2007, 7: 17-31.

[5] C. Luo, D.L. Ware, J.B. Zwischenberger, J.W. Clark, Jr., "A mechanical model of the human heart relating septal function to myocardial work and energy," *J Cardiovasc Engineering* 2008, 8: 174-84.

[6] C. Luo, D. Ramachandran, D.L. Ware, T.S. Ma, and J.W. Clark, Jr., "Modeling left ventricular diastolic dysfunction: classification and key indicators," *Theor Biol Med Model*, 2011, May 9; 8(1):14.

[7] E. Lim, A.H. Alomari, A.V. Savkin, and N.H. Lovell, "Noninvasive deadbeat control of an implantable rotary blood pump: a simulation study," *Proceedings of the 31st Annual Conference of the IEEE EMBS*, pp. 2855-2858, 2009.

[8] K. Furukawa, T. Motomura, and Y. Nose, "Right ventricular failure after left ventricular assist device implantation: the need for an implantable right ventricular assist device," *Artif Organs*, 2005, 29(5): 369-77.

[9] K. Chatterjee and B. Massie, "Systolic and diastolic heart failure: differences and similarities," *J Cardiac Failure*, 2007, 13(7): 569-576.

[10] S. Klotz, R.F. Foronjy, M.L. Dickstein, A. Gu, I.M. Garrelds, A.H.J. Danser, M.C. Oz, J. D'Armiento, D. Burkhoff, "Mechanical unloading during left ventricular assist device support increases left ventricular collagen cross-linking and myocardial stiffness," *Circulation*, 2005, 112: 364-374.

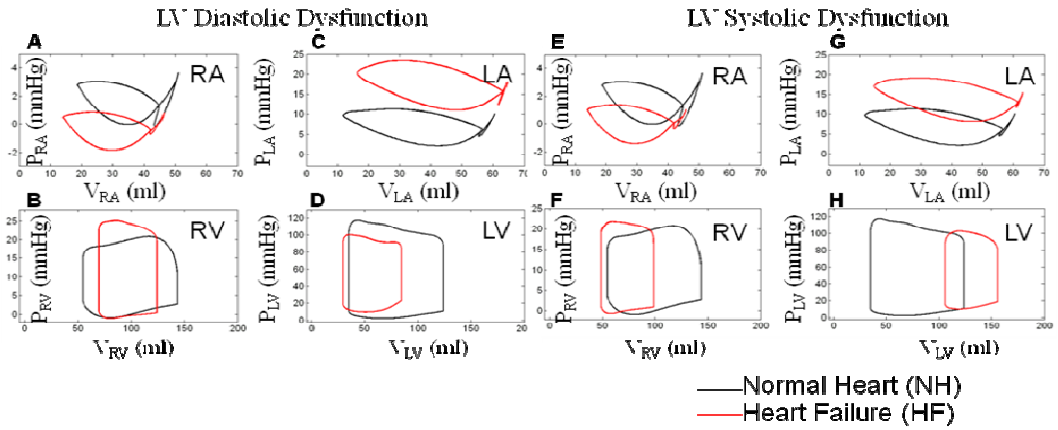

Fig. 1: Pressure-volume loops of the normal heart (black line) and diseased heart (red line). LVDD in Panels A-D and LVSD in Panels E-H.

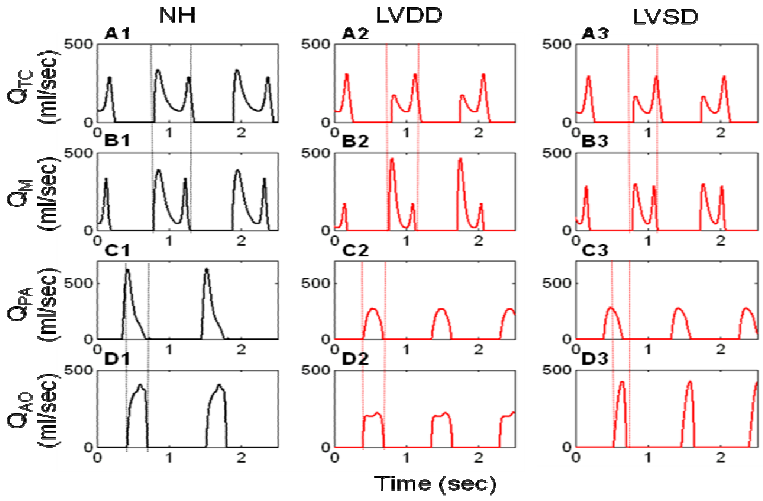

Fig. 2: Evaluation of ventricular mechanical dyssynchrony by way of observing the level of synchrony of inlet and outlet flows of the RV and LV. Normal heart (NH) is shown in Panels A1-D1. Transvalvular flows in LVDD (Panels A2-B2) are desynchronized in valve opening, with a tricuspid valve opening

delay, while the closure is like that of a normal heart (Panels A1-B1). Outlet flows are synchronized even at valve closure (Panels C2-D2), unlike the normal heart (Panels C1-D1). In the LVSD case, transvalvular flow synchrony matches that of a normal heart (Panels A3-B3), but the outlet flows are markedly desynchronized with a delayed opening of the aortic valve (Panel D3) and early closure of the pulmonic valve (Panel C3). LVDD is accompanied by transvalvular flow dyssynchrony, while LVSD is accompanied by output flow dyssynchrony.

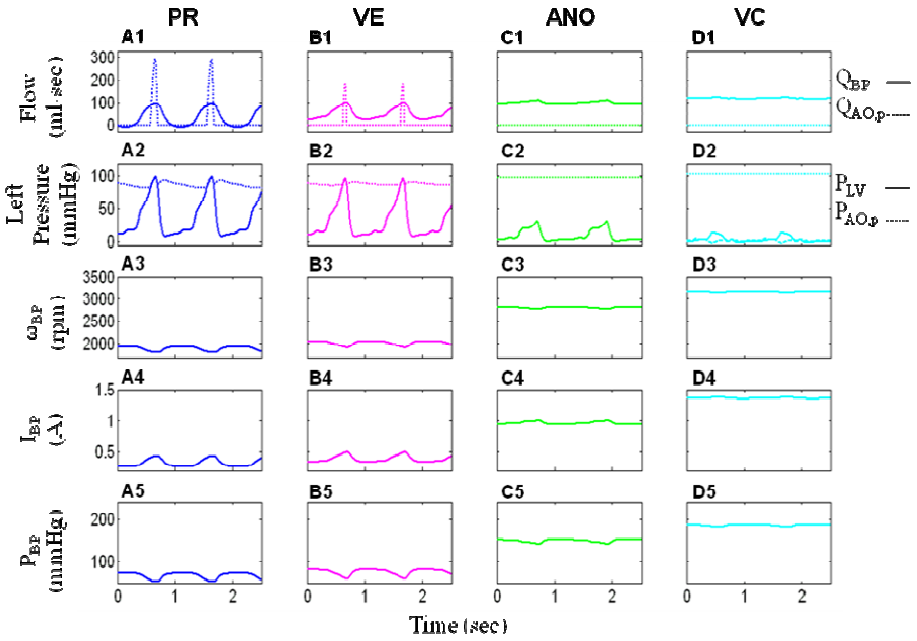

Fig. 3: After integration into the H-CRS model of LVSD, the iRBP's characteristic waveforms are shown, in four operating states: pump regurgitation (PR), ventricular ejection (VE), aortic valve does not open (ANO), and ventricular collapse (VC), at pump speeds 1950, 2000, 2800, and 3200 rpm, respectively. PR is seen with negative Q_{BP} (Panel A1). There is reduced LV outflow (Panel B1) and LV systolic contraction (Panel B2) in VE mode. Zero LV outflow (Panel C1) and lowered LV systolic pressures (Panel C2) are seen in ANO mode. VC is observed with a sharp drop in Q_{BP} at end-systole (Panel D1) coincident with negative P_{LV}. I_{BP} (Panels A4-D4) and P_{BP} (Panels A5-D5) steadily increase with increasing ω_{BP} (Panels A3-D3).

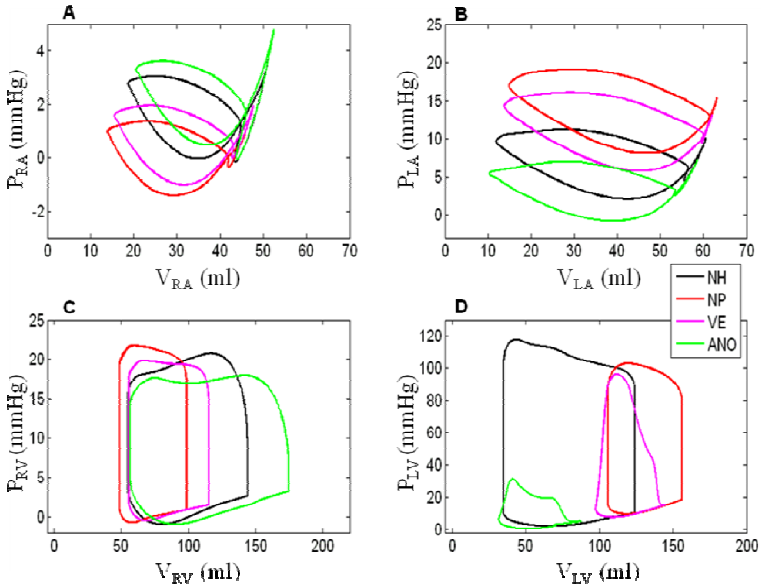

Fig. 4: Pressure-volume loops for all four chambers for four cases: NH, NP, VE, and ANO. With increasing pump speed, LV volume diminishes (Panel D), RV end-diastolic volume increases and systolic pressure increases (Panel C), RA pressure increases due to increased CO (Panel A), and LA pressure decreases due to lowered pulmonary congestion (Panel B).

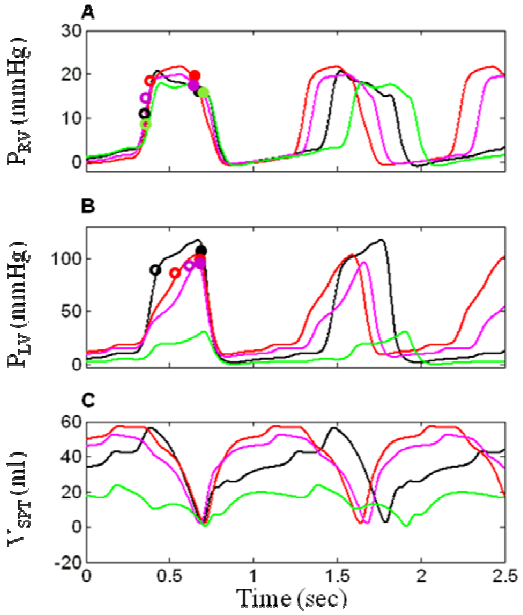

Fig. 5: RV and LV pressure are shown in Panels A and B, respectively, with open circles indicating outlet valve opening, and closed circles indicating outlet valve closure. Septal volume is shown in Panel C, where positive slope translates into rightward movement, and negative slope translates into leftward movement. With LVSD (red line), the septum is rightward bowed at early systole and septal priming stage disappears, delaying pulmonic valve opening (Panel A). The septum is delayed in its leftward thrust, prolonging LV contraction and delaying aortic valve opening. As speed increases, septal displacement diminishes, and in place of rightward movement during septal priming, the septum moves leftward. Septal aid to LV ejection worsens with further delayed leftward thrust.

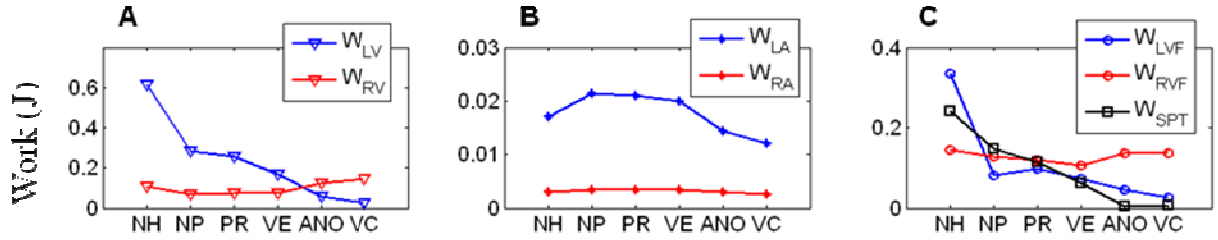

Fig. 6: Work done by individual components in the heart. Blue lines pertain to the left heart, red lines to the right heart, and black line to the septum. LV and LA work (W_{LV} and W_{LA}) shows decrease with increasing speeds. RV work (W_{RV}) tends to rise with increasing speeds, while W_{RA} remains relatively unaffected. LV free wall (W_{LVF}) and septal (W_{SPT}) work decrease to nearly zero while RV free wall (W_{RVF}) work tends to rise. NH=Normal heart, NP=R-type LVDD with no pump, PR=pump regurgitation, VE=ventricular ejection, ANO=aortic valve not open, VC=ventricular collapse.

Model Measurements of Key Indices

	LVET (sec)		RVET (sec)		HR (bpm)		SV (ml)		CO (L/min)		Heart Work (J)		Q_M E/A Ratio		Q_{TC} E/A Ratio	
	DD	SD	DD	SD	DD	SD	DD	SD	DD	SD	DD	SD	DD	SD	DD	SD
NH	0.28		0.34		55		89		4.9		1.46		1.15		1.12	
NP	0.29	0.18	0.27	0.26	63	64	55	50	3.5	3.2	0.81	0.74	2.67	1.05	0.57	0.56
PR	0.29	0.12	0.29	0.28	62	62	59	56	3.7	3.5	0.86	0.68	3.14	1.13	0.64	0.66
VE	0.06	0.07	0.33	0.29	56	60	80	60	4.5	3.6	0.59	0.51	1.58	0.94	0.87	0.70
ANO	0	0	0.37	0.38	50	50	113	118	5.7	5.9	0.44	0.39	1.20	0.86	1.19	1.33
VC	0	0	0.39	0.40	50	50	130	142	6.5	7.1	0.37	0.36	0.88	0.75	1.41	1.37

Table I: Key model measurements in LV diastolic dysfunction (DD) and systolic dysfunction (SD) simulations for normal heart (NH), LVSD with no pump (NP), pump regurgitation (PR), ventricular ejection (VE), aortic valve not open (ANO), and ventricular collapse (VC). LV ejection time (LVET) drops significantly with iRBP assistance, while RVET increases with pump speed. As speed increases, heart rate (HR) decreases, stroke volume (SV) increases and cardiac output (CO) increases. Heart work decreases with increasing speed. Mitral flow (Q_M) E/A ratio is abnormally high with LVDD and normal with LVSD, but decreases with pump speed, except with PR when the ratio increases. Q_{TC} E/A ratio is abnormally low in both LVDD and LVSD, but increases with pump speed.